

Effect of Thermal Annealing on the Electrochemical Capacitive Performance of Reduced Microcrystalline Graphene Oxide

*Yun Lei**, Zheng Zhang, Chengyi Fang, Xin Bing

School of Resources and Environmental Engineering, Wuhan University of Technology, Wuhan, 430070

*E-mail: leiyun@whut.edu.cn

Received: 9 June 2017 / Accepted: 3 August 2017 / Published: 12 September 2017

Microcrystalline graphene oxide (MGO) was reduced by thermal annealing to prepare reduced microcrystalline graphene oxide (RMGO). The produced RMGO was characterized by X-ray diffraction, ultraviolet-visible absorption spectroscopy, Fourier transform infrared spectroscopy and transmission electron microscopy. The results show that the absorption peaks of the oxygen-containing functional groups almost disappear due to the removal of oxygen atoms from the basal plane of graphene oxide in the temperature range of 150-450°C in nitrogen. The electrochemical behaviour of RMGO annealed at different temperature was evaluated by three-electrode cyclic voltammetry and electrochemical impedance spectroscopy. The results show that an obvious increase in specific capacitance and decrease in charge-transfer resistance can be observed for RMGO at the annealing temperature of 250°C.

Keywords: microcrystalline graphene oxide; graphene; thermal reduction; electrochemical properties

1. INTRODUCTION

Microcrystalline graphite, as a kind of resourceful and cheap graphite with a high degree of graphitization, consists of many microcrystals of different orientations [1]. To date, many reports have demonstrated the preparation of graphene from microcrystalline graphite garnering significant attention. Graphene, as a two-dimensional honeycomb lattice consisting of monolayer hexagonal carbon atoms, has attracted considerable interest recently because of its high theoretical specific surface area of 2630 m²g⁻¹ and excellent electronic conductivity and mechanical properties. These unique properties make it an ideal material for many potential applications [2-6]. Graphene can be prepared through several methods, such as mechanical exfoliation [7], solution-phase exfoliation [8],

electrochemical exfoliation [9], epitaxial growth [10], chemical vapour deposition [11], thermal and chemical reduction [12] and graphitization of silicon carbide [13]. Compared with these methods, thermal reduction is considered as one of the most effective methods for preparing graphene from GO. Peng et al. prepared graphene sheets from microcrystalline graphite by a low-temperature exfoliation method [14]. Chung et al. used rapid thermal annealing to control the quantity of oxygen functional groups attached on graphene oxide [15]. Ding et al. demonstrated effective two-step thermal annealing to significantly improve the C/O ratio in air at the relatively low temperature of 600°C [16]. Kumar et al. analysed electrical behaviour of amide-functionalized graphene oxide and graphene oxide films annealed at different temperatures [17]. Kim et al. investigated the remarkable conversion between n- and p-type reduced graphene oxide upon varying the thermal annealing temperature [18]. Zaumseil et al. demonstrated partial restoration of the graphene basal plane of rGO by annealing in Ar/H₂/isopropanol flow [19]. Yamaguchi et al. reported valence-band electronic structure evolution of graphene oxide upon thermal annealing for optoelectronics [20].

Herein, thermal reduction of microcrystalline graphene oxide was investigated in the temperature range of 150 - 450°C. The RMGO that was produced was characterized by X-ray diffraction, Fourier transform infrared spectroscopy, ultraviolet-visible absorption spectroscopy, and transmission electron microscopy. Meanwhile the electrochemical properties of RMGO were analysed by three-electrode cyclic voltammetry and electrochemical impedance spectroscopy.

2. EXPERIMENTAL

2.1. Materials

Microcrystalline graphite powders (99%), sulfuric acid (H₂SO₄), nitric acid (HNO₃), potassium permanganate (KMnO₄), sodium nitrate (NaNO₃), hydrogen peroxide (H₂O₂) and anhydrous ethanol (CH₃CH₂OH) were purchased from Sinopharm Chemical Reagent Co., Ltd.

2.2. Synthesis of microcrystalline graphite oxide and graphene oxide

Microcrystalline graphite oxide was prepared by the Hummers process including three stages of low, medium and high temperature. First, microcrystalline graphite was mixed with sodium nitrate and potassium permanganate at 0°C for 90 min. Second, the mixture was heated at 32-38°C for 30 min for further oxidation of the graphite intercalation compound. Lastly, hydrogen peroxide was added to the mixture, which was heated at 70-100°C for 15-20 min. The produced graphite oxide was further treated with ultrasonic oscillation to obtain graphene oxide. The product was rinsed with distilled water and dried in a vacuum oven at 45°C.

2.3. Preparation of reduced microcrystalline graphene oxide

Reduced microcrystalline graphene oxide was treated with thermal annealing at 150, 250, 350 and 450°C. In the thermal reduction process, reduced microcrystalline graphene oxide was placed in the centre of a quartz tube with nitrogen flow. As the tube furnace reached the annealing temperature of 150, 250, 350 or 450°C, reduced microcrystalline graphene oxide was annealed for 30 min. The products were denoted as RMGO-X, where “X” was the annealing temperature of 150, 250, 350 or 450°C.

2.4. Characterization

X-ray diffraction (XRD) was performed on a D/MX- III A diffractometer using the monochromatized X-ray beam from Cu K α radiation. UV-Vis adsorption spectra were obtained using a UV-Vis spectrophotometer (UV5500). Fourier transform infrared (FTIR) spectra were collected with a Nexus 670 FTIR spectrometer in the range of 400–4000 cm⁻¹ with a 1064 nm wavelength laser. The morphology of RMGO was observed on a JEM-2100F transmission electron microscopy (TEM). Cyclic voltammetry (CV) measurements and electrochemical impedance spectroscopy (EIS) measurements were carried out on a CHI650E electrochemical work station in a three-electrode system, which was equipped with a glassy carbon electrode coated with RMGO as the working electrode, a platinum foil as the counter electrode and a standard calomel electrode as the reference electrode. The electrochemical performance of RMGO was recorded at a scanning range from -0.55 to 0.55V in 0.1M H₂SO₄ solution at room temperature.

3. RESULTS AND DISCUSSION

3.1. XRD analysis

The XRD patterns of MGO and RMGO at different temperatures of 150, 250, 350 and 450°C are shown in Fig. 1. MGO presents a sharp diffraction peak at 2θ of 10.5°, attributed to the (001) lattice plane of GO. When MGO was annealed at different temperatures, the diffraction peak at 10.5° disappears due to the removal of oxygen atoms from the basal plane of graphene oxide. The presence of a broad diffraction peak at 23.4° means that MGO has been exfoliated from the raw graphite and reduced to graphene sheets during the annealing process. As the annealing temperature increases from 150 to 450°C, the broad diffraction peak slightly shifts from 23.4° to 25.6° due to the exfoliation of oxygen-containing groups on the graphene sheets. Kumar [17] also showed that the XRD pattern of graphene oxide gradually shifts to higher values when it is annealed at higher temperature.

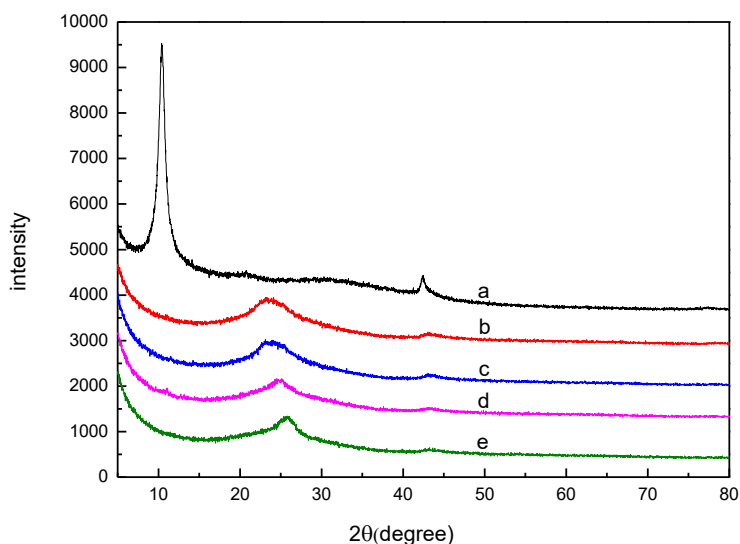


Figure 1. XRD patterns of MGO (a) and RMGO prepared with thermal annealing of 150 (b), 250 (c), 350 (d) and 450°C (e)

3.2 FTIR

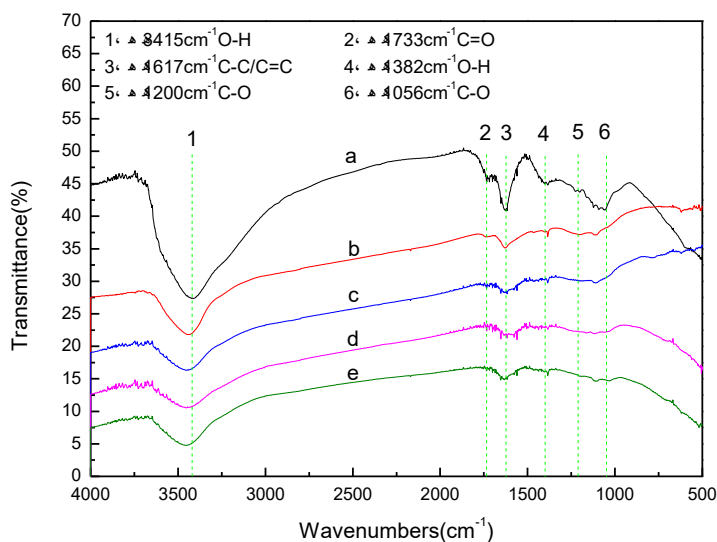


Figure 2. FTIR spectra of MGO (a) and RMGO prepared with thermal annealing of 150 (b), 250 (c), 350 (d) and 450°C (e)

Fig. 2 shows the FTIR transmission spectra of MGO and RMGO at reduction temperatures of 150, 250, 350 and 450°C. The FTIR spectrum of MGO exhibits absorption peaks at 1617 cm^{-1} corresponding to C-C/C=C stretching vibrations, 1723 cm^{-1} due to C=O stretching vibration, and 1056 and 1200 cm^{-1} ascribed to C-O symmetric and asymmetric stretching vibrations, respectively. The curve of MGO also exhibits broad absorption peaks centred at 3415 and 1382 cm^{-1} corresponding to

O-H stretching vibration of the hydroxyl group. As MGO was annealed at 150°C, the absorption peaks centred at 1733, 1382, 1200 and 1056 cm^{-1} corresponding to C=O, C-O and O-H are greatly weakened. The presence of weak absorption bands suggests the partial restoration of C sp^2 domains in the carbon basal plane. Upon further increasing the thermal reduction temperature from 150 to 450°C, the absorption peaks of the oxygen-containing functional groups almost disappear due to the removal of oxygen atoms from the basal plane of GO. During the annealing process in inert gas, most of the oxygen-containing functional groups can be removed when the temperature reaches 250°C, which is consistent with the results reported in the literature [21, 22].

3.3. UV-vis analysis

Fig.3 shows the UV-vis absorption spectra of MGO and thermally reduced MGO at different temperatures of 150, 250, 350 and 450°C. The absorption peak appears at 230 nm due to π - π^* transitions of aromatic C-C bonds and the shoulder at 308 nm corresponding to n - π^* transitions of C=O bonds. When MGO was thermally reduced at elevated temperature, the shoulder approximately 300 nm disappears due to the removal of oxygen containing functional groups. The absorption peak of RMGO shifts to 265nm corresponding to the excitation of π -plasmon of the graphitic structure. The results show that MGO has been thermally reduced to RMGO sheets due to the removal of C=O bonds in the temperature range of 150-450°C.

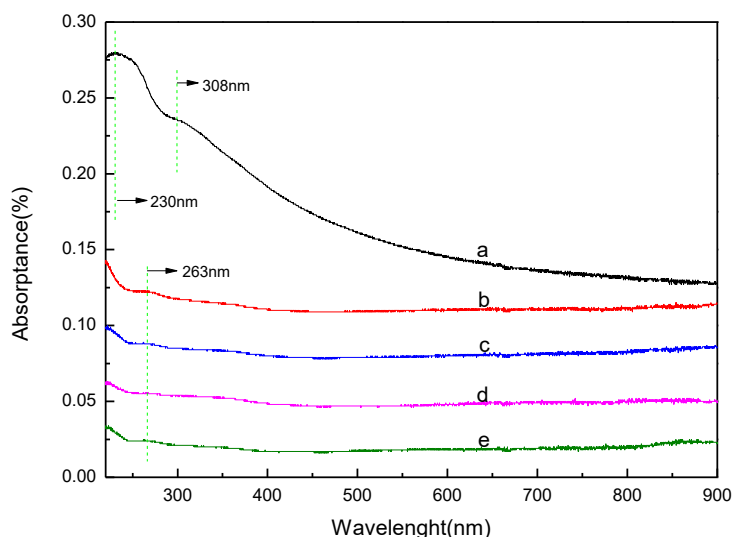


Figure 3. UV-visible spectra of MGO (a) and MRGO prepared with thermal annealing of 150 (b), 250 (c), 350 (d) and 450°C (e)

3.4 TEM

The morphology of RMGO was characterized by TEM analysis. As shown in Fig. 4, the graphene sheets have the two-dimensional structure with curled and corrugated wrinkles

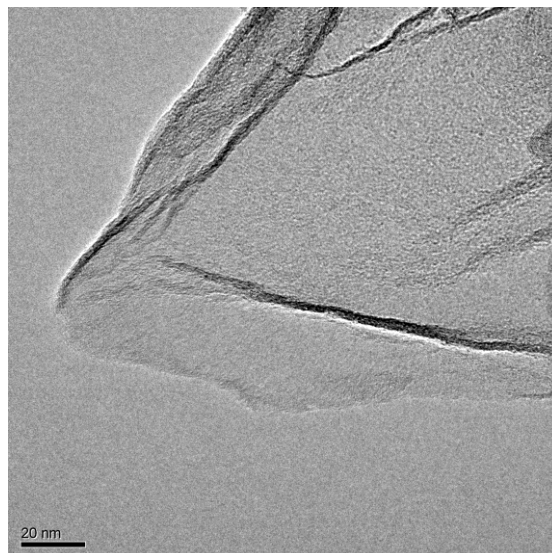


Figure 4. TEM image of reduced microcrystalline graphene oxide

3.5. CV

The electrochemical performance of RMGO at different annealing temperatures was evaluated by cyclic voltammetry within a potential range from -0.55 to 0.55V in 0.1M H₂SO₄ solution. The experimental data were collected after CV loops stabilized in the process of ten successive scanning cycles. Fig. 5a shows a comparison of CV curves for RMGO at temperatures of 150, 250, 350 and 450°C at a scan rate of 100mV/s. As the annealing temperature increases from 150 to 450°C, the current density of RMGO first increases, reaches a maximum at the temperature of 250°C, and then declines as the temperature increases further. Because high temperature causes explosive expansion and induces concentrated defects [23], low temperature is beneficial for the electrochemical performance of graphene sheets. CV curves show that an obvious increase in both the current density and specific capacitance can be observed for RMGO at the annealing temperature of 250°C.

The CV curves of RMGO150- RMGO450 were recorded at various scan rates of 5, 10, 20, 50 and 100mV/s. As shown in Fig. 5b-5e, the current density increases with increasing scan rate, which suggests the presence of ideal capacitive behaviour. The specific capacitance of RMGO can be calculated using the following equation:

$$C = \frac{1}{2v(V_f - V_i)m} \int_{V_i}^{V_f} I(V)dV$$

where C is the specific capacitance, (V_f - V_i) is the operating voltage range, m is the mass of active material in the electrode, v is the scan rate (mV/s), and $\int_{V_i}^{V_f} I(V)dV$ is the enclosed discharge area of the CV curve. The specific capacitance values of RMGO at different scan rates are shown in Fig. 5f and listed in Table 1. With the increase in scan rate, the capacitance decreases sharply at low scan rate and slightly at high scan rate, indicating that all of the RMGOs have good rate performance. Zhang [23] also showed that fewer oxygen groups remained on the surface of graphene and that the destroyed sp² system can be healed to some extent upon annealing, which gives recovery of the electrical conductivity of graphene sheets. As an improved electron transfer process, graphene sheets

can respond quickly to voltage changes, which result in a better rate performance. Fig. 5f shows a comparison of capacitance values upon increasing the scan rate from 5 to 100 mV/s. A higher specific capacitance and lower current density can be observed for RMGO at a lower scan rate. The changes may be attributed to the internal resistance of the electrode. When the scan rate is decreased, the lower current density leads to penetrating ions into the inner structure of electrode materials, which is favourable for the capacitive behaviour. While the scan rate is increased, the ions are limited to the outer surface of electrodes, which results in a decrease in the specific capacitance [24, 25].

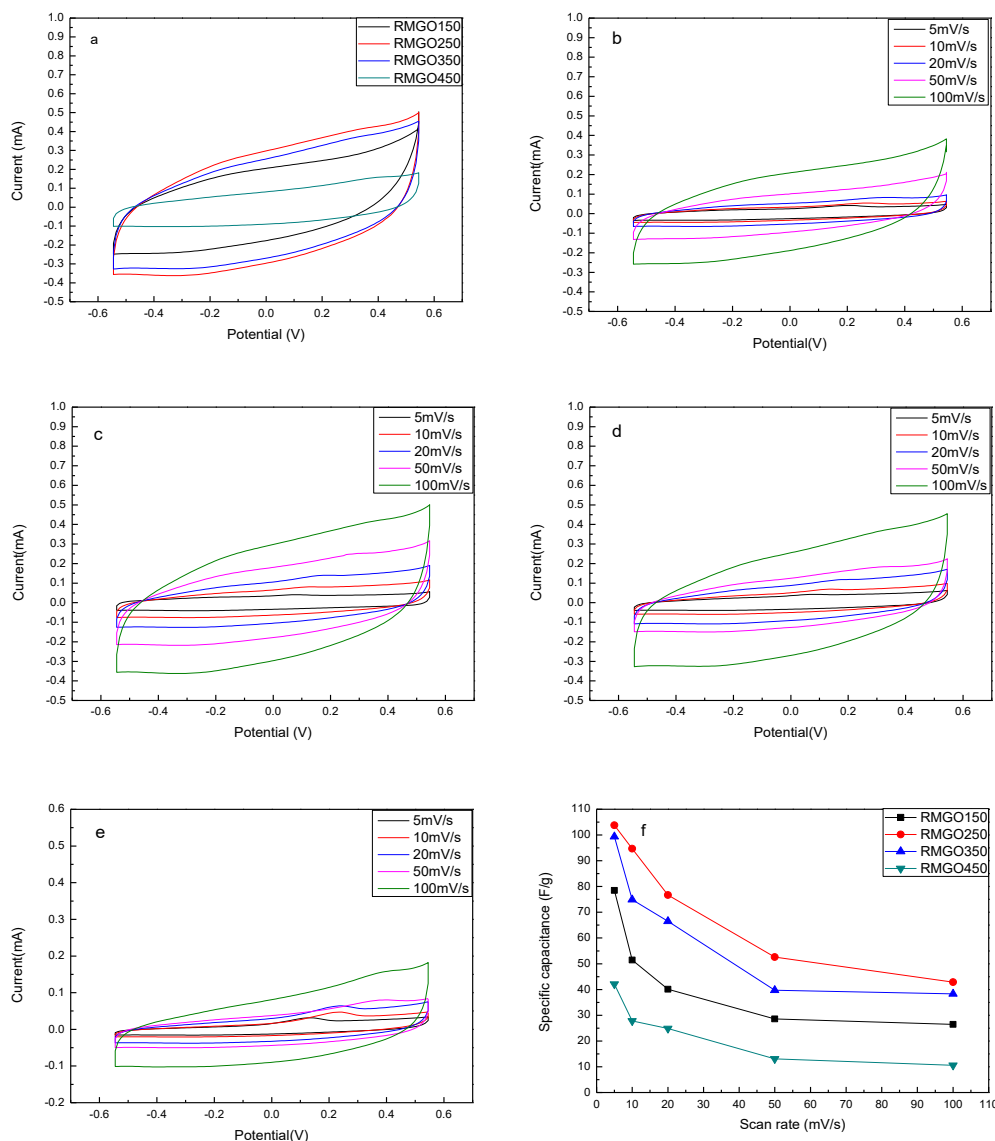


Figure 5. CV curves of RMGO prepared with different thermal annealing at a scan rate of 100mV/s (a). CV curves of RMGO-150 (b), RMGO-250 (c), RMGO-350 (d) and RMGO-450 (e) at different scan rates of 5, 10, 20, 50 and 100mV/s. (f) Specific capacitance values of RMGO150- RMGO450 at different scan rates of 5, 10, 20, 50 and 100mV/s.

Table 1. Specific capacitance values calculated from CV curves at the scan rate ranging from 5 to 100 mV/s

RMGO -X	Specific capacitance at different scan rate				
	5mV/s	10mV/s	20mV/s	50mV/s	100 mV/s
150°C	78.45	51.45	40.11	28.58	26.48
250°C	103.28	94.67	77.74	52.57	42.88
350°C	99.35	74.88	66.50	39.74	38.32
450°C	42.10	27.84	24.87	13.05	10.56

3.6. EIS

The electrochemical impedance of RMGO was investigated in the three-electrode systems. Fig. 7 displays the EIS Nyquist plots of RMGO at frequencies ranging from 1000 kHz to 0.1 Hz. All of the impedance plots are composed of a semicircle in high frequencies corresponding to the charge-transfer resistance occurring at the interface and a straight line in low frequencies related to the diffusion limited process. The arc radius on the EIS Nyquist plots of RMGO reaches the minimum at 250°C, which suggests that the more efficient transfer of charge carriers occurs on RMGO-250.

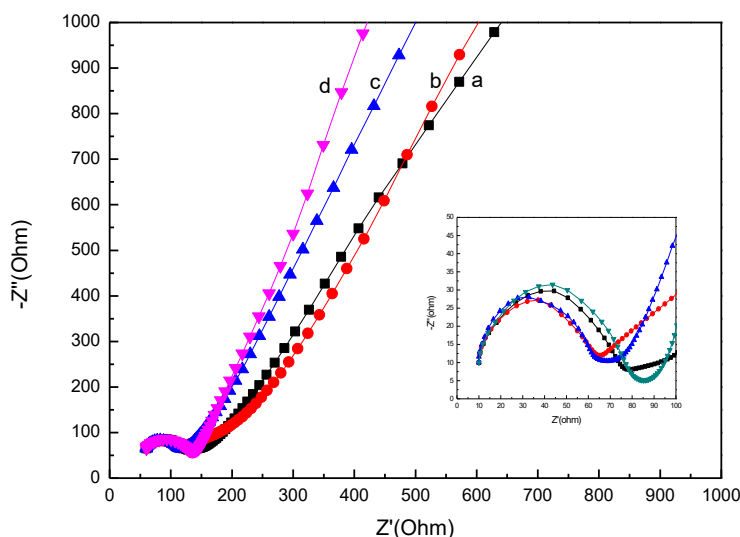


Figure 6. EIS of RMGO at thermal annealing of 150 (a), 250 (b), 350 (c) and 450°C (d)

4. CONCLUSIONS

In summary, MGO was treated with thermal annealing at temperatures of 150, 250, 350 and 450°C. The results show that MGO has been thermally reduced to RMGO sheets due to the removal of oxygen atoms from the basal plane of MGO in the temperature range of 150-450°C. The specific

capacitance of RMGO reaches a maximum of 103.28 F/g at 250°C, and the smaller semicircle arc suggests faster interfacial charge transfer occurs on RMGO-250.

ACKNOWLEDGMENTS

The work was supported by National Natural Science Foundation of China No. 51204129.

References

1. K. Li, K. Shen, Z. H. Huang, W. C. Shen, G. Z. Yang, J. H. Yang and F. Y. Kang, *Fuel*, 180 (2016) 743.
2. U. Saha, R. Jaiswal and T. H. Goswami, *Electrochim. Acta*, 196 (2016) 386.
3. Y. Lei, C. Y. Fang, J. Xu and Y. He, *Ceram. Int.*, 42 (2016) 5326.
4. R. Penu, A. C. Obreja, D. Patroi, M. Diaconu and G. L. Radu, *Microchem. J.*, 121 (2015) 130.
5. R. Bera, S. Kundu and A. Patra, *ACS Appl. Mater. Inter.*, 7 (2015) 13251.
6. H. Park, H. Ahn, Y. Chung, S. B. Cho, Y. S. Yoon and D. J. Kim, *Mater. Lett.*, 136 (2014) 164.
7. S. Fukada, Y. Shintani, M. Shimomura, F. Tahara and R. Yagi, *Jpn. J. Appl. Phys.*, 51 (2012) 085101.
8. T. C. Hernandez, A. C. F. Blanco, A. T. Williams, M. Velicky, H. V. Patten, A. Colina and R. A. W. Dryfe, *Electroanal.*, 27 (2015) 1026.
9. S. T. Hossain and R. G. Wang, *Electrochim. Acta*, 216 (2016) 253.
10. T. Rana, M. V. S. Chandrashekar, K. Daniels and T. Sudarshan, *J. Electron. Mater.*, 45 (2016) 2019.
11. B. Vasic, A. Zurutuza and R. Gajic, *Carbon*, 102 (2016) 304.
12. B. Dehghanzad, M. K. R. Aghjeh, O. Rafeie, A. Tavakoli and A. J. Oskooie, *Rsc Adv.*, 6 (2015) 3578.
13. H. J. Hwang, C. Cho, S. K. Lim, S. Y. Lee, C. G. Kang, H. Hwang and B. H. Lee, *Appl. Phys. Lett.*, 99 (2018) 082111.
14. H. Xian, T. Peng, H. Sun and J. D. Wang, *J. Mater. Sci.*, 50 (2015) 4025.
15. D. T. Phan and G. S. Chung, *Sensor. Actuat. B-Chem.*, 220 (2015) 1050.
16. S. Y. Tian, J. Sun, S. W. Yang, P. He, S. J. Ding, G. Q. Ding and X. M. Xie, *RSC Adv.*, 5 (2015) 69854.
17. S. Rani, M. Kumar, D. Kumar and S. Sharma, *Thin Solid Films*, 585 (2015) 13.
18. N. D. K. Tu, J. Choi, C. R. Park and H. Kim, *Chem. Mater.*, 27 (2015) 7362.
19. S. Grimm, M. Schweiger, S. Eigler and J. Zaumseil, *J. Phys. Chem. C*, 120 (2016) 3036.
20. H. Yamaguchi, S. Ogawa and D. Watanabe, *Phys. Status Solidi A*, 213(2016) 2380.
21. Y. Qiu, F. Guo, R. Hurt and I. Kulaots, *Carbon*, 72 (2014) 215.
22. M. Jin, H. K. Jeong, T. H. Kim, K. P. So, Y. Cui, W. J. Yu, E. J. Ra and Y. H. Lee, *J. Phys. D: Appl. Phys.*, 43 (2010) 275402.
23. C. Zhang, W. Lv, X. Y. Xie, D. M. Tang, C. Liu and Q. H. Yang, *Carbon*, 62 (2013) 11.
24. B. Wang, D. H. Guan, Z. Gao, J. Wang, Z. S. Li, W. L. Yang and L. H. Liu, *Mater. Chem. Phys.*, 141 (2013) 1.
25. H. Y. Xian, T. J. Peng, H. J. Sun and J. D. Wang, *J. Mater. Sci. - Mater. Electron.*, 26 (2015) 242.